

# Atomic States Entanglement in Carbon Nanotubes

I.V. Bondarev and B. Vlahovic  
Physics Department, North Carolina Central University,  
1801 Fayetteville Str, Durham, NC 27707, USA

A scheme for entangling atoms (ions) located close to or encapsulated inside a carbon nanotube is investigated using the photon Green function formalism for quantizing electromagnetic fields in the presence of quasi-one-dimensional absorbing and dispersing media. Small-diameter metallic nanotubes are shown to result in a high degree of the quantum bit entanglement for sufficiently long tubes.

PACS numbers: 78.40.Ri, 73.22.-f, 73.63.Fg, 78.67.Ch

In spite of impressive experimental demonstrations of basic quantum information effects in a number of different mesoscopic systems, such as quantum dots in semiconductor microcavities, cold ions in traps, nuclear spin systems, atoms in optical resonators, Josephson junctions, etc., their concrete implementation is still at the proof-of-principle stage (see, e.g., Ref. [1] for a review). The development of materials that may host quantum coherent states with long coherence lifetimes is a critical research problem for the nearest future [2]. There is a need for the fabrication of quantum bits (qubits) with coherence lifetimes at least three-four orders of magnitude longer than it takes to perform a bit ip. This would involve entangling operations, followed by the nearest neighbor interaction over short distances and quantum information transfer over longer distances. It is thus of vital importance to pursue a variety of different strategies and approaches towards physically implementing novel non-trivial applications in modern nanotechnology.

In this Letter, we study a scheme for entangling atoms (ions) located close to or encapsulated inside a carbon nanotube (CN). CNs are graphene sheets rolled-up into cylinders of approximately one nanometer in diameter. Extensive work carried out worldwide in recent years has revealed intriguing physical properties of these novel molecular scale wires [3]. Nanotubes have been shown to be useful for miniaturized electronic, mechanical, electromechanical, chemical and scanning probe devices and as materials for macroscopic composites [3, 4]. Recent experiments on the encapsulation of single atoms (ions) into single-walled CNs [5] and their intercalation into single-wall CN bundles [6], along with the progress in growth techniques of centimeter-long small-diameter single-walled CNs [7], stimulate the study of dynamic quantum coherent processes in atomically doped CNs.

It was shown recently that the relative density of photonic states (DOS) and the atom-vacuum-field coupling, respectively, near CNs effectively increase due to the presence of additional surface photonic modes coupled to CN electronic quasiparticle excitations [8]. In small-diameter CNs the strong atom-field coupling may occur [9, 10, 11] — the property that is known to facilitate the entanglement of spatially separated qubits [12,

13]. Qualitatively, in terms of the cavity quantum electrodynamics (QED), the coupling constant of an atom (modelled by a two-level system with the transition dipole moment  $d_A$  and frequency  $\omega_A$ ) to a vacuum field is given by  $hg = (2 d_A^2 \hbar \omega_A / \epsilon_0 V)^{1/2}$  with  $V$  being the effective volume of the field mode the atom interacts with (see, e.g., Ref. [14]). For the atom (ion) encapsulated into the CN of radius  $R_{cn}$ ,  $V = \pi R_{cn}^2 L$  ( $L = 2$ ) that is  $10^2 \text{ nm}^3$  for CNs with diameters  $\approx 1 \text{ nm}$  in the optical range of  $\omega_A \approx 600 \text{ nm}$ . Approximating  $d_A$  as  $e \hbar / m_A$  [15], one obtains  $hg \approx 0.3 \text{ eV}$ . On the other hand, the "cavity" linewidth is given for  $\omega_A$  in resonance with the cavity mode by  $\hbar \gamma_c = 6 \hbar c^3 / \omega_A^3 (Q_A) V$ , where  $Q_A$  is the atomic spontaneous emission enhancement/dehancement (Purcell) factor [14]. Taking into account large Purcell factors  $Q_A \approx 10^7$  close to CNs [8], one arrives at  $\hbar \gamma_c \approx 0.03 \text{ eV}$  for  $1 \text{ nm}$ -diameter CNs in the optical spectral range. Thus, for the atoms (ions) encapsulated into small-diameter CNs the strong atom-field coupling condition  $hg \approx \hbar \gamma_c$  is supposed to be satisfied, giving rise to the rearrangement ("dressing") of atomic levels and formation of atomic quasi-one-dimensional (1D) cavity polaritons [9, 10, 11]. The latter ones are similar to quasi-0D excitonic polaritons in quantum dots in semiconductor microcavities [16], that are currently being considered a possible way to produce the excitonic qubit entanglement [17]. Here we suggest an alternative way to generate the qubit entanglement by using quasi-1D atomic polariton states in CNs. We show that small-diameter metallic nanotubes result in sizable amounts of the two-qubit atomic entanglement. Envisaged applications of our scheme range from quantum information transfer over long distances (centimeter-long distances, as a matter of fact, since centimeter-long small-diameter single-walled CNs are now technologically available [7]) to novel sources of coherent light emitted by dopant atoms in CNs.

We use our previously developed photon Green function formalism for quantizing electromagnetic field close to quasi-1D absorbing and dispersing media [10, 11]. Representing such a medium, the (achiral) CN is considered to be an infinitely long, infinitely thin, anisotropically conducting cylinder. Its (axial) surface conductivity is

taken to be that given by the  $\pi$ -electron band structure in the tight-binding approximation with the azimuthal electron momentum quantization and axial electron momentum relaxation taken into account. Two identical two-level atoms, A and B, are supposed to be positioned at their respective equivalent places  $r_{A,B}$  close to the CN. We assign the orthonormal cylindrical basis  $f_{e_r}; e_{\phi}; e_z$  in such a way that  $e_z$  is directed along the nanotube axis and, without loss of generality,  $r_A = r_A e_r = fr_A; 0; 0$ ,  $r_B = fr_B; \phi_B; z_B$ . The atoms interact with a quantum vacuum electromagnetic field via their transition dipole moments that are assumed to be directed along the CN axis,  $d_{A,B} = d_z e_z$ . The contribution of the transverse dipole moment orientations is suppressed because of the strong depolarization of the transverse field in an isolated CN (the so-called dipole antenna effect [18]). We also assume the atoms to be located far enough from each other, to simplify the problem by ignoring the interatomic Coulomb interaction. The total secondly quantized Hamiltonian of the system is then given by [10, 11]

$$\hat{H} = \sum_{i=A,B} \int_{Z_1}^Z d\Omega \int_{\mathbb{R}^2} dR \hat{f}^\dagger(R; \Omega) \hat{f}(R; \Omega) + \sum_{i=A,B} \frac{\hbar t_i}{2} \hat{\Lambda}_i + \sum_{i=A,B} \int_{Z_1}^Z d\Omega \int_{\mathbb{R}^2} dR [g^{(+)}(r_i; R; \Omega) \hat{\Lambda}_i^{(+)}(r_i; R; \Omega) \hat{f}^\dagger(R; \Omega) + h.c.]; \quad (1)$$

where the three items represent the medium-assisted (modified by the presence of the CN) electromagnetic field, the two-level atoms, and their interaction with the medium-assisted field, respectively. The operators  $\hat{f}^\dagger(R; \Omega)$  and  $\hat{f}(R; \Omega)$  are the scalar bosonic field operators defined on the CN surface assigned by the radius-vector  $R = fr_{cn}; \phi; z$  with  $r_{cn}$  being the radius of the CN. These operators create and annihilate the single-quantum bosonic-type electromagnetic medium excitation of the frequency  $\Omega$  at the point  $R$  of the CN surface. The Pauli operators,  $\hat{\Lambda}_i = \hat{J}_i \hat{u}_i \hat{J}_i$ ,  $\hat{\Lambda}_i^{(+)} = \hat{J}_i \hat{u}_i \hat{L}_i \hat{J}_i$  and  $\hat{\Lambda}_i = \hat{J}_i \hat{u}_i \hat{L}_i \hat{J}_i$  with  $i = A$  or  $B$ , describe the atomic subsystem and electric dipole transitions between its two states, upper  $\hat{J}_i \hat{u}_i$  with either of the two atoms in its upper state and lower  $\hat{J}_i \hat{L}_i$  with both atoms in their lower states, separated by the transition frequency  $\Omega_A$ . This (bare) frequency is modified by the diamagnetic ( $A^2$ ) atom-field interaction yielding the new renormalized transition frequency  $t_i = \Omega_A [1 - 2(\hbar \Omega_A)^2 \sum_{\mathbb{R}^2} \int_{Z_1}^Z d\Omega \int_{\mathbb{R}^2} dR \hat{J}_i^{\dagger 2}(r_i; R; \Omega) \hat{J}_i^2]$  in the second term of the Hamiltonian. The dipole atom-field interaction matrix elements are given by  $g^{(+)} = g^2 (\Omega = \Omega_A) g^k$  where  $g^{2(k)} = \frac{i(4\Omega_A = c^2)^2}{\hbar} \text{Re} \int_{Z_1}^Z d\Omega \int_{\mathbb{R}^2} dR G_{zz}^{(k)}(r_i; R; \Omega)$  with  $G_{zz}^{(k)}(r_i; R; \Omega)$  being the  $zz$ -component of the transverse (longitudinal) Green tensor (with respect to the first variable) of the electromagnetic subsystem and  $\int_{Z_1}^Z d\Omega$  representing the CN surface axial conductivity. The matrix elements  $g^{2(k)}$  have the property of

$\int_{\mathbb{R}^2} dR \hat{J}_i^{\dagger 2}(r_i; R; \Omega) \hat{J}_i^2 = (\hbar^2 = 2 \int_{\mathbb{R}^2} d\Omega) (\Omega_A = \Omega)^2 \int_{Z_1}^Z d\Omega \int_{\mathbb{R}^2} dR G_{zz}^{(k)}(r_i; R; \Omega) G_{zz}^{(k)}(r_i; R; \Omega) = \text{Im} \int_{\mathbb{R}^2} dR G_{zz}^{(k)}(r_i; R; \Omega) = \text{Im} G_{zz}^{(k)}(\Omega)$  being the transverse (longitudinal) local photonic DOS functions and  $\int_{Z_1}^Z d\Omega \int_{\mathbb{R}^2} dR G_{zz}^{(k)}(\Omega) = 8 \int_{\mathbb{R}^2} d\Omega \int_{Z_1}^Z dR \text{Im} G_{zz}^{(k)}(\Omega) = 3\hbar c^2$  representing the atomic spontaneous decay rate in vacuum where  $\text{Im} G_{zz}^{(k)}(\Omega) = \Omega = 6 \text{ c}$  is the vacuum imaginary Green tensor  $zz$ -component. The Hamiltonian (1) involves only two standard approximations: the electric dipole approximation and the two-level approximation. The rotating wave approximation commonly used is not applied, and the diamagnetic term of the atom-field interaction is not neglected (as opposed to, e.g., Refs. [8, 9]).

For single-quantum excitations, the time-dependent wave function of the whole system can be written as

$$|j(t)\rangle = \sum_{i=A,B} C_{U_i}(t) e^{i(t_i - T)t} \hat{J}_i |i\rangle |f_0\rangle |0\rangle + \int_{\mathbb{R}^2} dR \sum_{i=A,B} C_L(R; \Omega; t) e^{i(\Omega - T)t} \hat{J}_i |i\rangle |R; \Omega\rangle |i\rangle; \quad (2)$$

where  $T = \sum_{i=A,B} t_i = 2$ ,  $|f_0\rangle$  is the vacuum state of the field subsystem,  $|f_1(R; \Omega)\rangle$  is its excited state with the field being in the single-quantum Fock state,  $C_{U_i}$  and  $C_L$  are the respective probability amplitudes of the upper states and the lower state of the system. For the following it is convenient to introduce the new variables  $C(t) = [C_{U_A}(t) C_{U_B}(t)]^T = \frac{1}{\sqrt{2}}$  that are the expansion coefficients of the wave function (2) in terms of the maximally entangled 2-qubit atomic states  $|j_i\rangle = (|j_A i\rangle |j_B i\rangle) = \frac{1}{\sqrt{2}}$ . In view of Eqs. (1) and (2), the time-dependent Schrödinger equation yields then

$$i \dot{C}(t) = \int_{\mathbb{R}^2} d\Omega K(\Omega) C(t) + f(t); \quad (3)$$

where

$$K(\Omega) = \int_{\mathbb{R}^2} d\Omega \int_{Z_1}^Z dx \frac{\tilde{\chi}_0(x)}{2} (r_A; r_B; x) e^{i(x - x_A)\Omega} |0\rangle; \quad (4)$$

$$(r_A; r_B; x) = \frac{x_A^2}{x^2} \int_{Z_1}^Z d\Omega G_{zz}^{(k)}(r_A; x) \int_{Z_1}^Z d\Omega G_{zz}^{(k)}(r_A; r_B; x) + \int_{Z_1}^Z d\Omega G_{zz}^{(k)}(r_A; x) \int_{Z_1}^Z d\Omega G_{zz}^{(k)}(r_A; r_B; x); \quad (5)$$

$$f(t) = \frac{1}{\sqrt{2}} \int_{\mathbb{R}^2} d\Omega K(\Omega) C_{U_A}(\Omega) |0\rangle; \quad (6)$$

and we have, for convenience, introduced the dimensionless variables  $\tilde{\chi}_0 = \hbar \Omega_0 = 2 \Omega_0$ ,  $x = \hbar \Omega = 2 \Omega_0 t$ , and  $\Omega = 2 \Omega_0 t = \hbar$  with  $\Omega_0 = 2.7 \text{ eV}$  being the carbon nearest neighbor hopping integral ( $\hbar = 2 \Omega_0 = 1.22 \cdot 10^{16} \text{ s}$ ) appearing in the CN surface axial conductivity  $\int_{Z_1}^Z d\Omega$ . The functions  $f(t)$  are only unequal to zero when the two atoms are initially in their ground states, with the initial excitation residing in the nanotube. Eq. (6) assumes that this situation is realized by selecting the time origin to be right after the time interval  $\tau$ , that is necessary for the (excited) atom A to

decay completely into the nanotube photonic modes, has elapsed. The two-particle local photonic DOS functions  $\rho^{(k)}(r_A; r_B; \mathbf{x}) = \text{Im} \rho^{(k)} G_{zz}^{(k)}(r_A; r_B; \mathbf{x}) = \text{Im} G_{zz}^0(\mathbf{x})$  are the generalizations of the DOS functions  $\rho^{(k)}(r_A; \mathbf{x})$  (see Refs. [10, 11]). They are of the form  $\rho^{(k)} = 1 + \rho^{(k)}$ ,  $\rho^{(k)} = -k$  with the medium-dependent contributions given for  $r_A, r_B < R_{cn}$  by

$$\rho^{(k)}(r_A; r_B; \mathbf{x}) = \frac{3}{4} \text{Im} \int_{\mathcal{C}} e^{ip'r_B} \frac{Z}{C} dy \frac{v^4}{y^2 v^2} s(R_{cn}; \mathbf{x}) \quad (7)$$

$$\frac{K_p^2 [v(R_{cn}; \mathbf{x})] I_p [v(r_A; \mathbf{x})] I_p [v(r_B; \mathbf{x})] \cos[u(z_B; \mathbf{x})y]}{1 + s(R_{cn}; \mathbf{x}) v^2 I_p [v(R_{cn}; \mathbf{x})] K_p [v(R_{cn}; \mathbf{x})]};$$

where  $I_p$  and  $K_p$  are the modified cylindrical Bessel functions,  $v(y) = \sqrt{y^2 - 1}$ ,  $u(r) = 2.0 r = hc$ , and  $s(R_{cn}; \mathbf{x}) = 2i u(R_{cn}; \mathbf{x}) \bar{\chi}_{zz}(R_{cn}; \mathbf{x})$  with  $\bar{\chi}_{zz} = 2 h_{zz} = e^2$  being the dimensionless CN surface conductivity per unit length and  $e^2 = hc = 1/137$  representing the fine-structure constant. The integration contour  $\mathcal{C}$  goes along the real axis of the complex plane and envelopes the branch points  $y = \pm 1$  of the function  $v(y)$  in the integrands from below and from above, respectively. For  $r_A, r_B > R_{cn}$ , Eq. (7) is modified by the replacement  $r_A, r_B \rightarrow R_{cn}$  in the Bessel function arguments in the numerator of the integrand.

The entanglement of two quantum bits occurs when the 2-qubit wave function cannot be represented as a product of the two 1-qubit states in any basis. To determine this quantity in our particular case, we follow the recipe based on the "spin flip" transformation and valid for an arbitrary number of qubits (see Ref. [19] for details). First, we define the reduced density matrix  $\hat{\rho}_{AB}(\rho) = \text{tr}_{\mathcal{H}_{AB}}(\rho) = \text{tr}_{\mathcal{H}_{AB}}(\rho)$  describing the bipartite atomic subsystem in terms of the wave function (2) of the whole system. Next, we introduce the "concurrence"  $C(\rho_{AB}) = \sqrt{\lambda_{\max}(\tilde{\rho}_{AB})}$  where  $\tilde{\rho}_{AB} = \sqrt{\rho_{AB}} \sqrt{\rho_{AB}}$  with  $\sqrt{\rho_{AB}}$  being the Pauli matrix that represents the "spin flip" transformation in the atom A (B) single-qubit space. This, after some algebra, becomes  $C(\rho_{AB}) = \sqrt{2 \sqrt{1 - \mathcal{C}(\rho_{AB})^2}}$  with  $\mathcal{C}(\rho_{AB})$  given by the integral equation (3). Finally, the degree of the entanglement of the 2-qubit atomic state  $\rho_{AB}$  is given by  $E(\rho_{AB}) = \max\{0, \mathcal{C}(\rho_{AB})\}^2 = 2g$  where  $h(y) = y \log_2 y - (1-y) \log_2 (1-y)$ .

The entanglement  $E(\rho_{AB})$  is maximal when the coefficients  $C_+(\rho)$  and  $C(\rho)$  are maximally different from each other. For this to occur, the functions  $\rho(r_A; r_B; \mathbf{x})$  in Eqs. (3)-(6) should be different in their values. These are determined by  $\rho^{(k)}(r_A; r_B; \mathbf{x})$  whose frequency behavior is determined by the CN surface axial conductivity  $\chi_{zz}$ . We computed  $\rho^{(k)}$  from Eq.(7) with  $\chi_{zz}$  calculated beforehand in the relaxation-time approximation (relaxation time  $3 \times 10^{-12}$  s [20]) at temperature 300 K [9, 10, 11]. Then, the integral equation was solved

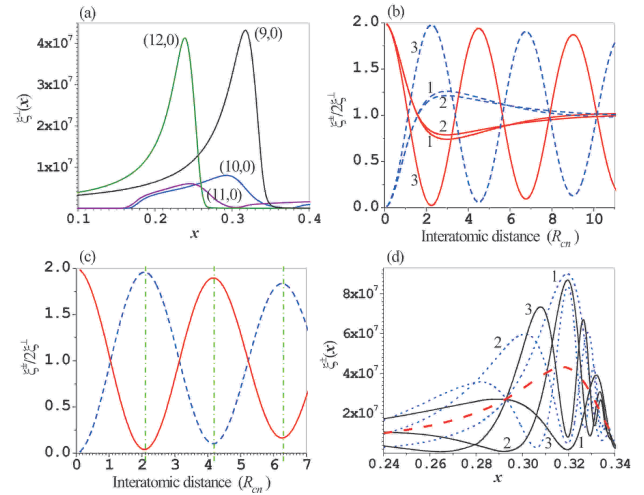


FIG. 1: (Color online) (a) Transverse local photonic DOS functions  $\rho^{(k)}(x)$  for the two-level atom in the centers of the four 'zigzag' nanotubes. (b) Normalized two-particle local photonic DOS functions  $\rho^{(k)}(x)$  (solid lines) and  $\rho^{(k)}(x)$  (dashed lines) taken at the peak frequencies of  $\rho^{(k)}(x)$  [see (a)], as functions of the distances between the two atoms on the axes of the (10,0) (lines 1;  $x = 0.29$ ), (11,0) (lines 2;  $x = 0.25$ ) and (12,0) (lines 3;  $x = 0.24$ ) CNs. (c) Same as in (b) for the two atoms on the axis of the (9,0) CN ( $x = 0.32$ ). (d) Two-particle DOS functions  $\rho^{(k)}(x)$  (solid lines) and  $\rho^{(k)}(x)$  (dotted lines) for the two atoms located in the center of the (9,0) CN and separated from each other by the distances of  $2.1R_{cn} = 7.4 \text{ \AA}$  (lines 1),  $4.2R_{cn} = 14.8 \text{ \AA}$  (lines 2) and  $6.3R_{cn} = 22.2 \text{ \AA}$  (lines 3) [shown by the vertical lines in (c)]; the dashed line shows  $\rho^{(k)}(x)$  for the atom in the center of the (9,0) CN.

numerically to obtain  $C(\rho)$  and  $E(\rho_{AB})$ . The vacuum spontaneous decay rate was estimated from the expression  $\gamma_0(x) \propto x^3$  valid for atomic systems with Coulomb interaction [15]. The atomic transition frequency  $\omega_A$  was assumed to be  $\omega_x$ , the local DOS resonance frequency. The simplest, most interesting case was considered where both of the atoms are positioned in the center of the CN.

Shown in Fig. 1 (a) is a typical frequency behavior of the one-particle transverse photonic DOS  $\rho^{(k)}(r_A = 0; \mathbf{x})$  in the infrared and visible frequency range  $x < 0.4$  for the atom inside 'zigzag' CNs of increasing radii. The DOS resonances are seen to be much sharper for metallic CNs ( $m = 3q$ ;  $q = 1; 2; \dots$ ) than for semiconducting ( $m \notin 3q$ ) in agreement with the fact that this frequency range is dominated by the classical Drude-type conductivity which is larger in metallic CNs [8]. Figure 1 (b) shows the normalized two-particle local photonic DOS functions  $\rho^{(k)}(x)$  taken at the resonance frequencies of the respective  $\rho^{(k)}$ 's [Fig. 1 (a)], as functions of the distance between the two atoms on the axes of the (10,0), (11,0) and (12,0) CNs. The values of  $\rho^{(k)}$  and  $\rho^{(k)}$  are seen to be substantially different from each other before they reach

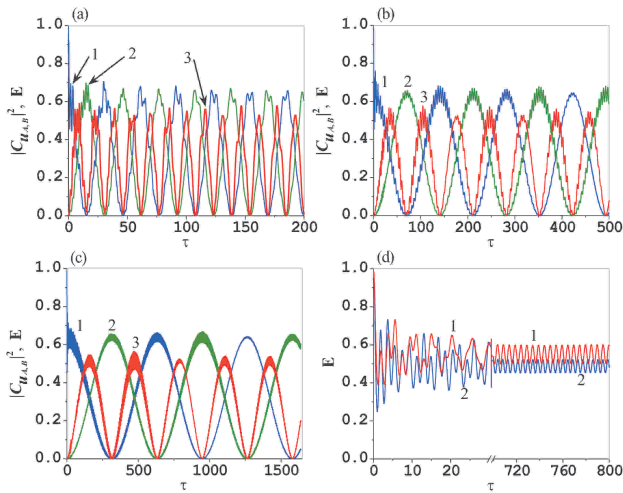


FIG. 2: (Color online) (a), (b), (c) Upper decay of the initially excited atom A (lines 1) and initially unexcited atom B (lines 2), and the entanglement (lines 3), as functions of dimensionless time for the two atoms located in the center of the (9,0) CN and separated from each other by the distances of  $2.1R_{cn}$  (7.4 Å),  $4.2R_{cn}$  (14.8 Å) and  $6.3R_{cn}$  (22.2 Å), respectively [the situation shown in terms of local photonic DOS in Figs. 1 (c), (d)]. (d) Short-time and long-time entanglement evolution of the initially fully entangled atoms separated by 7.4 Å; lines 1 and 2 are for  $C_+(0) = 1; C_-(0) = 0$  and  $C_+(0) = 0; C_-(0) = 1$ , respectively.

their limit values of  $\rho^+ = \rho^- + \rho^k - 2\rho^?$  at sufficiently large interatomic separations. For metallic CNs the functions  $\rho^+$  and  $\rho^-$  exhibit resonator-like behavior, i.e. they vary periodically in antiphase almost without damping with increasing interatomic separation. In Fig. 1 (c) is shown the dependence of  $\rho^?$  ( $x = 0.32$ ) [peak position of  $\rho^?$  in Fig. 1 (a)] on the interatomic separation for the atoms in the center of the metallic (9,0) CN. As the separation increases,  $\rho^+$  and  $\rho^-$  may differ greatly one from another in a periodic way. The maximal difference is  $\rho^+ - \rho^- = 2(\rho^? + \rho^k) - 4\rho^? - 10\rho^?$ , making the mixing coefficients  $C_{\pm}$  different and thus resulting in a substantial degree of the entanglement of the two spatially separated atomic qubits. Figure 1 (d) gives an example of the frequency behavior at  $x = x_c = 0.32$  for the three interatomic distances [shown by the vertical lines in Fig. 1 (c)] corresponding to "antinode" relative positioning of the atoms in the center of the (9,0) CN.

The ensuing spontaneous decay dynamics and atomic entanglement are presented in Fig. 2 for the atoms in the center of the (9,0) CN. In (a), (b), (c) atom A is supposed to be initially excited while atom B is in its ground state. The entanglement is seen to reach the amount of 0.5 and to vary with time periodically without damping at least for the (reasonably long) times we restricted ourselves in our computations. As the interatomic separation increases, so the period of the entanglement oscillations

does while no change occurs in the maximal entanglement. In (d) both of the atoms are initially maximally entangled [ $C_+(0) = 1$  while  $C_-(0) = 0$ ] and separated by the distance of 7.4 Å. The entanglement is slightly larger in the case where  $C_+(0) = 1; C_-(0) = 0$  and no damping occurs as before. Note that the atoms can be separated by longer distances with roughly the same entanglement due to the periodicity with interatomic distance.

We have demonstrated sizable amounts of the two-qubit atomic entanglement in small-diameter metallic CNs. The entanglement greatly exceeds 0.35 that is known to be the maximal value one can achieve in the weak atom-field coupling regime [13], and persists with no damping for very long times. We attribute such a behavior to the strong atom-field coupling and electronic structure resulting in the resonator-like distance dependence of the two-particle local DOS in metallic CNs. The scheme studied can be generalized to the multi-atom entanglement via the nearest neighbor pairwise quantum correlations, thus challenging novel applications of atomically doped CNs in quantum information science.

This work was supported by NSF (ECS-0631347), DOD (W 911NF-05-1-0502) and NASA (NAG 3-804) grants. Discussions with M. Gelin are gratefully acknowledged.

Also at: Institute for Nuclear Problems, Belarusian State University, Bobruiskaya Str. 11, 220050 Minsk, Belarus

- [1] T. Brandes, Phys. Rep. 408, 315 (2005).
- [2] A. S. Sørensen et al., Phys. Rev. Lett. 92, 063601 (2004).
- [3] H. Dai, Surf. Sci. 500, 218 (2002).
- [4] R. H. Baughman, A. A. Zakhidov, and W. A. de Heer, Science 297, 787 (2002).
- [5] G.-H. Jeong et al., Phys. Rev. B 68, 075410 (2003); Thin Solid Films 435, 307 (2003); M. Khazaei et al., J. Phys. Chem. B 108, 15529 (2004).
- [6] L. Duclaux, Carbon 40, 1751 (2002); H. Shimoda et al., Phys. Rev. Lett. 88, 015502 (2002).
- [7] S. M. Huang, B. M. Aynor, X. Y. Cai, and J. Liu, Advanced Materials, 15, 1651 (2003); L. Zheng et al., Nature Materials, 3, 673 (2004).
- [8] I. V. Bondarev et al., Phys. Rev. Lett. 89, 115504 (2002).
- [9] I. V. Bondarev and Ph. Lambin, Phys. Rev. B 70, 035407 (2004); Phys. Lett. A 328, 235 (2004).
- [10] I. V. Bondarev and Ph. Lambin, Phys. Rev. B 72, 035451 (2005); Solid State Commun. 132, 203 (2004).
- [11] I. V. Bondarev and Ph. Lambin, in: Trends in Nanotubes Research (Nova Science, New York, 2006).
- [12] J. I. Cirac et al., Phys. Rev. Lett. 78, 3221 (1997).
- [13] H. T. Dung et al., J. Opt. B 4, S169 (2002).
- [14] L. C. Andreani, G. Panzarini, and J.-M. Gerard, Phys. Rev. B 60, 13276 (1999).
- [15] A. S. Davydov, Quantum Mechanics (NEO, Ann Arbor, MI, 1967).
- [16] J. P. Reithmaier et al., Nature 432, 197 (2004); T. Yoshie et al., ibid. 432, 200 (2004); E. Peter et al., Phys. Rev. Lett. 95, 067401 (2005).
- [17] S. Hughes, Phys. Rev. Lett. 94, 227402 (2005).

[18] A Jorio et al, Phys. Rev. B 65, 121402R (2002).  
[19] W K Wootters, Phys. Rev. Lett. 80, 2245 (1998).

[20] S J Tans et al, Nature 386, 474 (1997).